UNIVERSITY OF BIRMINGHAM
University of Birmingham Research at Birmingham

Four volcanically driven climatic perturbations led to enhanced continental weathering during the Late Triassic Carnian Pluvial Episode

Zhang, Peixin; Yang, Minfang; Lu, Jing; Jiang, Zhongfeng; Vervoort, Pam; Zhou, Kai; Xu, Xiaotao; Chen, Huijuan ; Wang, Ye; He, Zhen; Bian, Xiao; Shao, Longyi; Hilton, Jason

DOI:
10.1016/j.epsl.2023.118517

License:
Creative Commons: Attribution (CC BY)

Document Version
Publisher's PDF, also known as Version of record

Citation for published version (Harvard):
Zhang, P, Yang, M, Lu, J, Jiang, Z, Vervoort, P, Zhou, K, Xu, X, Chen, H, Wang, Y, He, Z, Bian, X, Shao, L & Hilton, J 2024, 'Four volcanically driven climatic perturbations led to enhanced continental weathering during the Late Triassic Carnian Pluvial Episode', *Earth and Planetary Science Letters*, vol. 626, 118517. https://doi.org/10.1016/j.epsl.2023.118517

Link to publication on Research at Birmingham portal

General rights
Unless a licence is specified above, all rights (including copyright and moral rights) in this document are retained by the authors and/or the copyright holders. The express permission of the copyright holder must be obtained for any use of this material other than for purposes permitted by law.

•Users may freely distribute the URL that is used to identify this publication.
•Users may download and/or print one copy of the publication from the University of Birmingham research portal for the purpose of private study or non-commercial research.
•User may use extracts from the document in line with the concept of 'fair dealing' under the Copyright, Designs and Patents Act 1988 (?)
•Users may not further distribute the material nor use it for the purposes of commercial gain.

Where a licence is displayed above, please note the terms and conditions of the licence govern your use of this document.

When citing, please reference the published version.

Take down policy
While the University of Birmingham exercises care and attention in making items available there are rare occasions when an item has been uploaded in error or has been deemed to be commercially or otherwise sensitive.

If you believe that this is the case for this document, please contact UBIRA@lists.bham.ac.uk providing details and we will remove access to the work immediately and investigate.

Download date: 06. May. 2024

Earth Planet. Sci. Lett. 626 (2024) 118517

Contents lists available at ScienceDirect

Earth and Planetary Science Letters

journal homepage: www.elsevier.com/locate/epsl

Four volcanically driven climatic perturbations led to enhanced continental weathering during the Late Triassic Carnian Pluvial Episode

Peixin Zhang [a,b], Minfang Yang [c], Jing Lu [a,*], Zhongfeng Jiang [b], Pam Vervoort [d], Kai Zhou [e], Xiaotao Xu [f], Huijuan Chen [b], Ye Wang [a], Zhen He [a], Xiao Bian [a], Longyi Shao [a], Jason Hilton [d,g,*]

[a] State Key Laboratory of Coal Resources and Safe Mining, College of Geoscience and Surveying Engineering, China University of Mining and Technology, Beijing 100083, China
[b] Henan International Joint Laboratory of Green Low Carbon Water Treatment Technology and Water Resources Utilization, School of Municipal and Environmental Engineering, Henan University of Urban Construction, Pingdingshan, Henan 467036, China
[c] Research Institute of Petroleum Exploration and Development, Petro China, Beijing 100083, China
[d] School of Geography, Earth and Environmental Sciences, University of Birmingham, Edgbaston, Birmingham B15 2TT, UK
[e] State Key Laboratory of Hydroscience and Engineering, Department of Hydraulic Engineering, Tsinghua University, Beijing 100084, China
[f] General Prospecting Institute of China National Administration of Coal Geology, Beijing 100038, China
[g] Birmingham Institute of Forest Research, University of Birmingham, Edgbaston, Birmingham B15 2TT, UK

ARTICLE INFO

Keywords:
Late Triassic
Carnian Pluvial Episode
Continental chemical weathering
Paleoclimate
North China

ABSTRACT

The arid climate of the Late Triassic was interrupted by a particularly humid episode known as the Carnian Pluvial Episode (CPE; ca. 234–232 million years ago). The CPE is often linked to eruptions in the Wrangellia Large Igneous Province (LIP), and is assumed to have led to global warming, enhanced weathering, water deoxygenation, and biotic changes. However, direct evidence for a temporal link between volcanic activity and chemical weathering has not yet been established due to the lack of comprehensive records across the CPE. In this study, geochemical and mineralogical analyses are applied to a lacustrine stratigraphic succession of the Jiyuan Basin (North China) that captures the CPE in high resolution. We identify four distinct pulses of enhanced continental chemical weathering characterized by elevated Chemical Index of Alteration values and kaolinite contents. These peaks in continental weathering coincide with Hg/TOC enrichments and negative organic carbon isotope excursions that mark four short (~400 kyr) but intense pulses of Wrangellia LIP volcanism. In combination with signs of increased humidity, our findings provide direct and independent evidence that Wrangellia LIP eruptions significantly altered CPE chemical weathering rates in response to global warming and wetting. The lake experienced eutrophication and water deoxygenation after each volcanic pulse but the swift recovery of carbon isotopes suggests that the system rapidly returned to conditions prior to the volcanic perturbation. Organic carbon burial facilitated by widespread dysoxic and anoxic waters, and CO_2 consumption via enhanced weathering likely played crucial roles in the rapid climatic recovery after each volcanic pulse.

1. Introduction

The Late Triassic Carnian Pluvial Episode (CPE; ca. 234–232 Ma) was an interval associated with biotic extinctions, species turnover, and the radiation of many new lineages of dinosaurs, mammals, insects and families of modern conifers (Simms and Ruffell, 1989; Dal Corso et al., 2020). It was first recognised as a particularly humid episode that starkly contrasted with the prevailing arid conditions of the Triassic (Simms and Ruffell, 1989). In addition to the evidence for increased rainfall and intensification of the hydrological cycle (Simms and Ruffell, 1989; Kozur and Bachmann, 2010; Dal Corso et al., 2018), paleorecords later also demonstrated that the CPE coincides with an increase in global temperature (Hornung et al., 2007a; Trotter et al., 2015; Sun et al., 2016; Dal Corso et al., 2022), multiple negative carbon isotope excursion (CIEs) (Sun et al., 2016; Miller et al., 2017; Dal Corso et al., 2018, 2020; Lu et al., 2021; Tomimatsu et al., 2021; Li et al., 2022), the shutdown of marine carbonate platforms (Hornung et al., 2007b; Jin et al., 2020), ocean and lake anoxia (Sun et al., 2016; Lu et al., 2021), and intensification of continental weathering (Rostási et al., 2011; Dal Corso et al., 2015; Baranyi et al., 2019a; Pecorari et al., 2023).

* Corresponding authors.
E-mail addresses: lujing@cumtb.edu.cn (J. Lu), j.m.hilton@bham.ac.uk (J. Hilton).

https://doi.org/10.1016/j.epsl.2023.118517
Received 21 August 2023; Received in revised form 21 November 2023; Accepted 23 November 2023
Available online 14 December 2023
0012-821X/© 2023 The Author(s). Published by Elsevier B.V. This is an open access article under the CC BY license (http://creativecommons.org/licenses/by/4.0/).

The leading hypothesis for the origin of the CPE is that volcanic eruptions and the associated release of CO_2 from the Wrangellia Large Igneous Province (LIP) caused global warming and intensified the hydrological cycle (Dal Corso et al., 2012; Lu et al., 2021; Mazaheri-Johari et al., 2021; Zhao et al., 2022; Jin et al., 2023). Multiple sequential negative CIEs recorded at various sites (Dal Corso et al., 2015, 2018, 2020; Sun et al., 2016; Miller et al., 2017; Lu et al., 2021; Tomimatsu et al., 2021; Li et al., 2022) suggest pulsed releases of isotopically light carbon, each likely of volcanic origin and less than 400 kyr in duration (Lu et al., 2021). Remarkably, the isotopic recoveries appear to be geologically rapid which strongly implies the importance of organic carbon burial in each recovery stage potentially facilitated by the

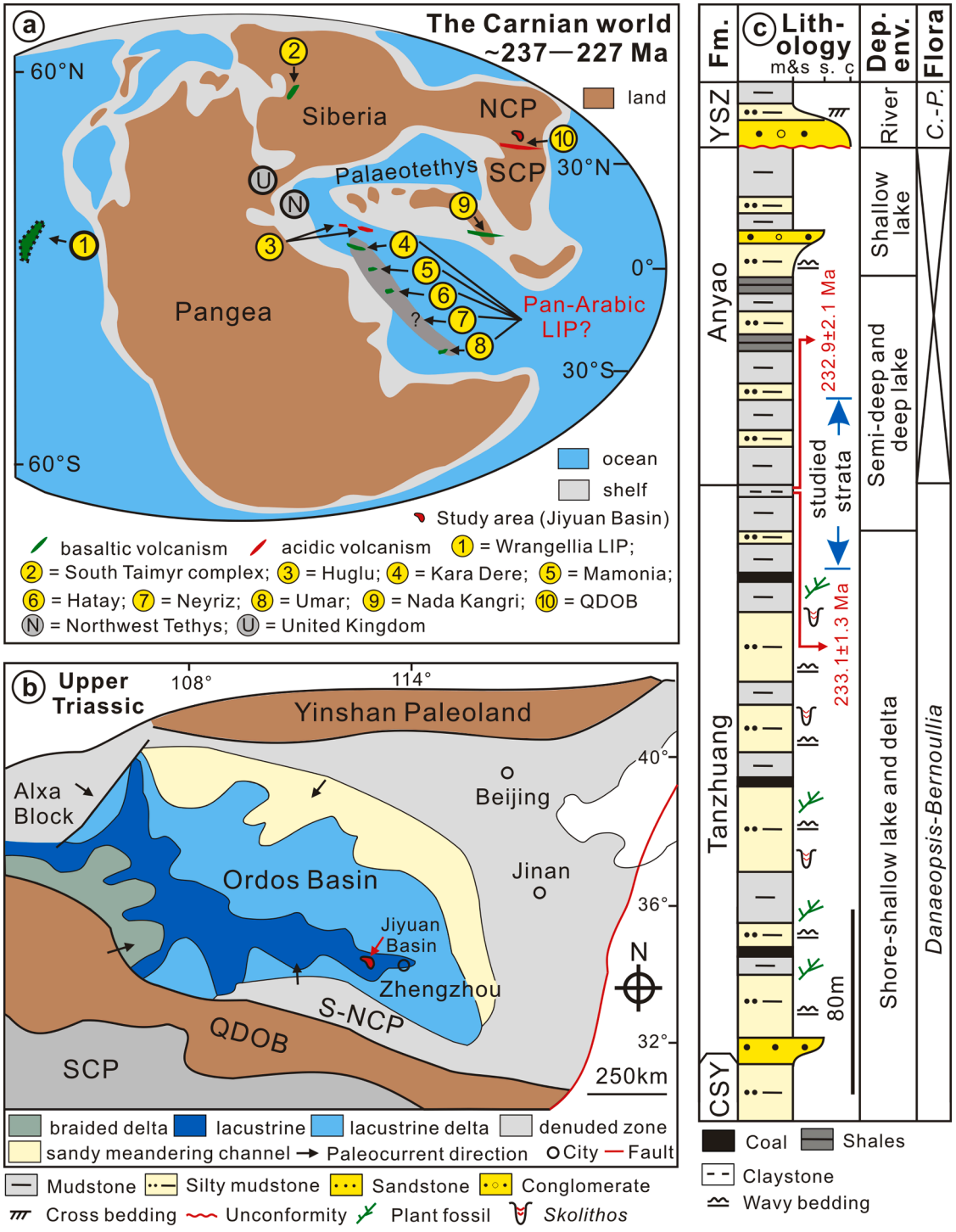

Fig. 1. Location and geological context for the study area. (a) Global paleogeographic reconstruction of the Carnian Stage (~237 to 227 Ma, Late Triassic), showing locations of the study area and volcanic centers (revised after (Lu et al., 2021)). (b) Tectono-paleogeographic map of the North China Plate during the Late Triassic (modified from (Liu et al., 2013)), showing the location of the study area. (c) Stratigraphic framework of the Upper Chunshuyao Formation (CSY) to the Lower Yangshuzhuang (YSZ) Formation from the Jiyuan Basin (modified from (Lu et al., 2021)). Abbreviations: LIP = Large Igneous Province; QDOB = Qingling-Dabie Orogenic Belt; S-NCP = southern NCP; SCP = South China Plate; Fm. = Formation; m & *s*= mudstone, and silty mudstone; s. = sandstone; *c*= conglomerate; Dep. env. = Depositional environment; *C.-P.* = *Coniopteris-Phoenicopsis*.

presence of widespread anoxia (Sun et al., 2016; Dal Corso et al., 2020; Lu et al., 2021; Tomimatsu et al., 2021). Enhanced continental chemical weathering may have played a key role in accelerating terrestrial runoff and nutrient input that drove water deoxygenation and enhanced organic carbon burial, providing a negative feedback to the initial volcanic outgassing (Shen et al., 2022; Yang et al., 2022). This hypothesis, however, relies heavily on the link between Wrangallia volcanism and weathering that has not yet been definitively shown due to the lack of high-resolution records across the CPE (e.g., Dal Corso et al., 2020). Identifying this link is key for our understanding of how the Late Triassic Earth systems responded to the volcanic release of CO_2 and pinpoint the processes that drove subsequent climate and recovery.

Here, we examine borehole ZJ-1 in the Jiyuan Basin from the southern part of the North China Plate (NCP) to reconstruct continental chemical weathering and climatic changes through the CPE using high-resolution geochemical and mineralogical analyses. We combined these data with previously published U-Pb dates, palynological analysis, and other geochemical proxies from the same borehole, including $\delta^{13}C_{org}$ values, Hg/TOC ratio, P/Al ratio, and Th/U ratio (Lu et al., 2021), to reveal potential temporal links between the Wrangellia LIP, continental chemical weathering, and climatic perturbations.

2. Geological setting

During the Late Triassic, the NCP was located at approximately 30–40°N in the Eastern Tethys (Liu et al., 2013) (Figs. 1a, b). The Yinshan palaeoland lay to the north, the Qinling-Dabie Orogenic Belt (QDOB) to the south, and the Ordos Basin occupied the NCP interior (Liu et al., 2013) (Fig. 1b). At this time the Jiyuan Basin was a sub-basin in the larger Ordos Basin, located in its southeastern area (Liu et al., 2013) (Fig. 1b). Sediments in the Jiyuan Basin were mainly derived from the northern QDOB and the southern NCP (Yang et al., 2012) (Fig. 1b).

The stratigraphic succession of rock types and fossil plant assemblages from the Late Triassic to Middle Jurassic in the Jiyuan Basin is shown in Fig. 1c. At the bottom of the succession, the Tanzhuang Formation consists mainly of grey and grey-green silty mudstones with grey-white thin sandstones and thin coal seams, and grey-white aluminous claystones at the top. Sediments of the Tanzhuang Formation were deposited in shore-shallow lake and delta to semi-deep and deep lake environments (Lu et al., 2021) (Fig. 1c). The Anyao Formation conformably overlays the Tanzhuang Formation and is primarily composed of grey and grey–black shales, intercalated with thin layers of turbidite sandstone deposited in semi-deep and deep lacustrine and shore-shallow environments (Lu et al., 2021; Zhang et al., 2022a) (Fig. 1c). At the top of the stratigraphic succession, the Yangshuzhuang Formation conformably overlies the Anyao Formation. It comprises gray-white thick sandstones and gray-green mudstones deposited in fluvial environments (Lu et al., 2021) (Fig. 1c). The geochronology of the target strata in this study from the upper part of Tanzhuang Formation to lower part of the Anyao Formation is based on previous results from zircon U-Pb dating, chemostratigraphy ($\delta^{13}C_{org}$ patterns), and palynological biostratigraphy, that constrained it to the Carnian stage of the Late Triassic (Lu et al., 2021) (Fig. 1c).

3. Materials and methods

From borehole ZJ-1 in the Jiyuan Basin, 55 fresh mudstone samples (sampling locations shown in Fig. 2) were collected from the Tanzhuang to the Anyao formations. Each sample was crushed into particles approximately 200 μm or less in diameter and then divided into three parts for analysis of (1) major elements, (2) trace elements, and (3) clay mineral compositions.

Major and trace elements were measured at the Beijing Research Institute of Uranium Geology with an X-ray fluorescence spectrometer (PW2404) and an inductively coupled plasma mass spectrometer (Element XR), respectively. The spectrometer was calibrated before use

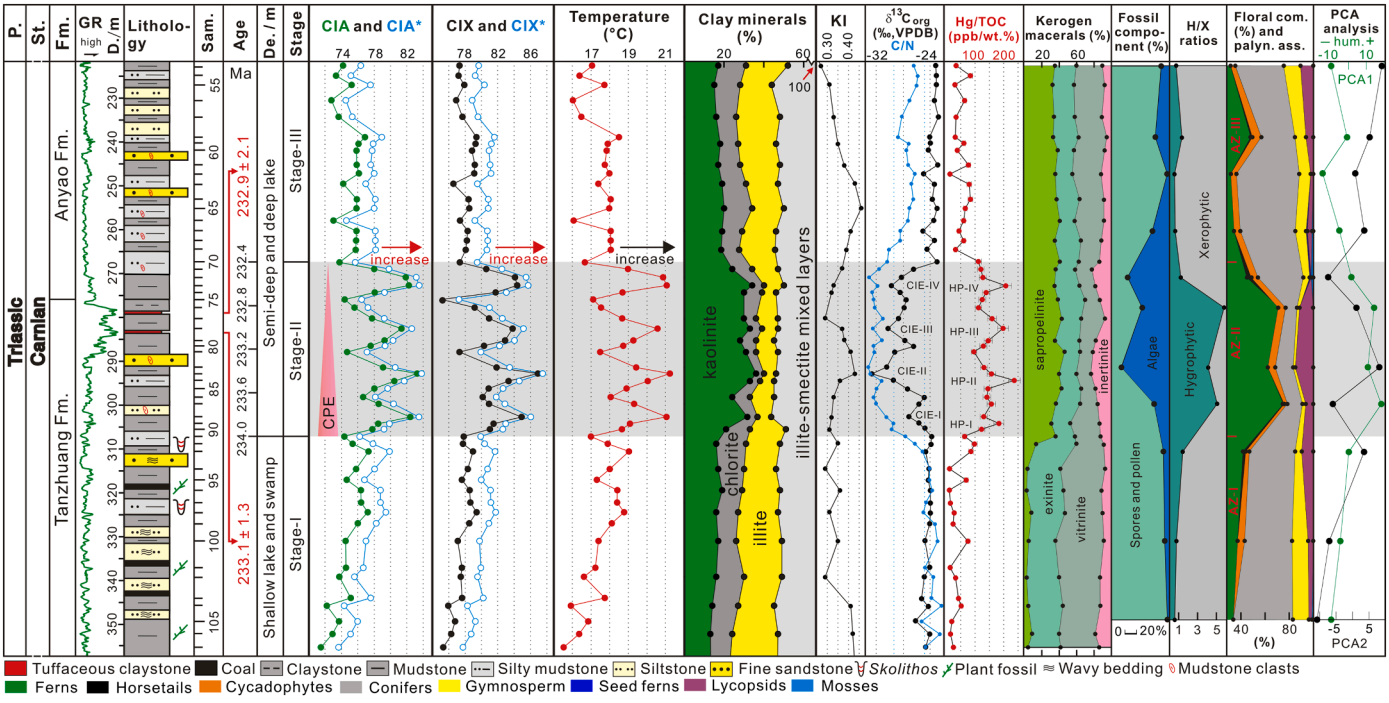

Fig. 2. Results of CIA (CIA*) values, CIX (CIX*) values, WIP (WIP*) values, temperature, clay mineral compositions, illite crystallinity (KI) values, $\delta^{13}C_{org}$ values, Hg/TOC ratios, kerogen macerals, fossil component, hygrophytic/xerophytic (H/X) ratios, floral composition and palynology assemblage zone, and principal components analysis (PCA) from the studied ZJ-1 borehole in the Jiyuan Basin. Abbreviations: P. = Period; St. = Stage; Fm. = Formation; GR = natural gamma-ray curves; D. = Deep; Sam. = Sample; De. = Depositional environment; VPDB = Vienna Pee Dee Belemnite; CIE-I to CIE-IV = from the first organic CIE to the fourth organic CIE; HP-I to HP-IV = from the first Hg/TOC peak to the fourth Hg/TOC peak; Floral com. (%) and palyn. ass. = Floral composition (%) and palynology assemblage; AZ = assemblage zone; hum. = humidity.

with standards of China National Certified Reference Material soil (GBW07427) and has an analytic precision within 5 %. Clay mineral composition was analysed using an X-ray diffractometer (D/max 2500 PC) at the State Key Laboratory of Coal Resources and Safe Mining (Beijing), and the data were interpreted using Clayquan 2016 software with a relative analysis error of ±5 %. The analytic precision or error of all samples is based on reproducibility and repeats of the standard sample and standard samples were run after every five sample analyses.

The weathering indices, including the Chemical Index of Alteration (CIA) and corrected CIA (CIA*), Chemical Index of Alteration without CaO (CIX) and corrected CIX (CIX*), Chemical Index of Weathering (CIW), Weathering Index of Parker (WIP) and corrected CIW (WIP*), and sodium depletion index (τNa) values, were calculated to quantify the intensity of subaerial chemical weathering (these weathering indices were calculated according to the formulae outlined in the Supplementary Material). Paleoclimate inferences have been recovered from CIA values, with climate sensitive spore-pollen fossils and kaolinite content used for reference (e.g., Lu et al., 2021; Zhang et al., 2023a). The relationship between the CIA and land surface temperatures were estimated according to the formula outlined in the Supplementary Material.

In addition, we performed statistical analysis on the palynological data in our section to further assess the environmental affinity (temperature rather than humidity) of palynological assemblages. Principal Components Analysis (PCA) by CANOCO software (Lepš and Šmilauer, 2003) was performed to transform the relative abundances of spore-pollen taxa vertically through the sedimentary succession into climatic parameters including temperature and humidity (e.g., Baranyi et al., 2019a, 2019b; Zhang et al., 2023b). Spore and pollen data were ordinated using non-metric multidimensional scaling (nMDS) ordination analysis with the Bray–Curtis similarity matrix (at two dimensions; conducted using the PAST v3.11 software) (Hammer et al., 2001). This ordination method detects patterns of co-occurrence among taxa as well as ecological gradients (e.g., Slater et al., 2019; Zhang et al., 2023b). The results and discussion of these analyses are included in the Supplementary Material.

4. Results

4.1. Geochemical compositions

The Geochemical and clay mineral composition and various indices of chemical weathering, including the CIA, CIX, CIW, WIP, and τNa values of mudstone (Nesbitt and Young, 1984; Fedo et al., 1995; Huang et al., 2017; Zhang et al., 2023a), were used to reconstruct the weathering trends of the parent rock in the provenance area (See Materials and Methods, Fig. 2, and Table S1). In this study, Al_2O_3 contents vary from 9.1 to 21.7 % ($\bar{x}$ = 15.2 %), SiO_2 contents vary from 32.1 to 59.6 % ($\bar{x}$ = 47.3 %), and Al/Si ratios range between 0.12 and 0.32 % ($\bar{x}$ = 0.19) (Table S1). All samples deviate from the ideal weathering trend line on the A-CN-K diagram in the study area (Fig. S1a), suggesting that K-metasomatism has some influence on the sediment (Fedo et al., 1995; Lu et al., 2020). This can cause lower CIA values and higher WIP values, but will not affect τNa and CIW values (Yang et al., 2022). Therefore, we corrected for K-metasomatism according to the method proposed by predecessors (Fedo et al., 1995; Huang et al., 2017) and calculated the CIA*, CIX*, and WIP* (See Materials and Methods, Table S2). Furthermore, we used the background values in the average source rock from the southern NCP (Gao et al., 1998) to calculate the changes in τNa and the A-CN-K trend in the studied Jiyuan Basin that arise from the sediment influx of southern NCP origin (Yang et al., 2012).

The CIA* values vary from 73.6 to 83.8 ($\bar{x}$ = 78.2), WIP* values from 25.5 to 54.4 ($\bar{x}$ = 44.0), CIX* values range between 77.2 and 87.5 ($\bar{x}$ = 81.3), CIW values between 86.6 and 94.8 ($\bar{x}$ = 91.1), and the τNa values vary from −0.86 to −0.54 ($\bar{x}$ = −0.72) (Fig. 2, Table S2). Across the CPE, four distinct peaks in CIA* and CIX* can be identified that occur synchronously with negative organic carbon isotope ($\delta^{13}C_{org}$) excursions (CIEs) (Fig. 2). The $\delta^{13}C_{org}$ values (Lu et al., 2021) vary from −32.7 to −22.8‰ ($\bar{x}$ = −25.1‰) and show four negative organic CIEs across the CPE with amplitudes of −3.4‰ (CIE-I), −7.8‰ (CIE-II), −3.8‰ (CIE-III), and −2.2‰ (CIE-IV) in samples 70 to 91 (Fig. 2). Extrapolating the sedimentation rate (25 m/Ma) between the two U–Pb ages (233.1 ± 1.3 Ma and 232.9 ± 2.1 Ma) to the entire succession (Lu et al., 2021) yields approximate durations of ~370 kyr (CIE-I), ~470 kyr (CIE-II), ~390 kyr (CIE-III), and ~370 kyr (CIE-IV), respectively. In a previous study (Lu et al., 2021), we found that Hg shows stronger covariation with TOC (r = +0.89) than with Al (r = +0.33) or total sulfide (r = +0.38), suggesting that Hg is mostly hosted by organic matter. Therefore, we can use the Hg/TOC values to normalize the Hg concentration. The Hg/TOC ratio varies from 10.79 to 236.97 ppb/wt % ($\bar{x}$ = 84.16 ppb/wt %), showing a pattern similar to the Hg concentrations with four pronounced peaks in samples 70 to 91 that have a distribution that is broadly anticorrelated with $\delta^{13}C_{org}$ (Fig. 2).

4.2. Clay mineral compositions and illite crystallinity

Results of clay mineral compositions and illite crystallinity (Kübler Index, KI) are shown in Figures 2, S2, and Table S3. Clay mineral compositions mainly comprise of illite-smectite mixed layers ($\bar{x}$ = 52.9 %), followed by kaolinite ($\bar{x}$ = 22.2 %) and illite ($\bar{x}$ = 15.1 %), with infrequent chlorite ($\bar{x}$ = 9.8 %) (Fig. 2). The content of the illite-smectite mixed layers varies from 48 to 56 %, illite from 6 to 23 %, and chlorite concentrations vary from 4 to 15 % (Fig. 2). Kaolinite content varies from 13 to 36 % and has significantly higher contents from samples 71 to 91, roughly corresponding to the CIA* peaks (Fig. 2). KI values vary from 0.27 to 0.42 % ($\bar{x}$ = 0.36Δ°/2θ) (Fig. 2).

4.3. Paleoclimatological inferences of palynological assemblages

A total of 26 spores genera, 28 pollen genera and 5 algae genera have been identified in the study section (Lu et al., 2021). They are assigned to three palynological assemblage zones (AZ) based on palynomorph abundance variations (Fig. 2; Lu et al., 2021). The compositions of AZ-I and AZ-III are broadly similar: gymnosperm pollen dominate, followed by fern spores, with a few algae present. In contrast, AZ-II is algae dominated together with fern spores, whilst gymnosperm pollen is less abundant (Fig. 2; Lu et al., 2021). Notably, an increase of spores relative to pollen abundance, with a significant increase in *Alisporites*, is also recorded in the Carnian terrestrial Dunscombe Mudstone in southwest England, where it coincides with a rise of freshwater algae and is interpreted as evidence for lake expansion during the CPE (Baranyi et al., 2019a).

According to the climatic affinity of the palynological fossils, the spores and pollen identified were classified into hygrophytes and xerophytes. We follow previous studies in which all spores are classified as hygrophytes together with *Alisporites, Aulisporites*, and Cycadopites groups, and all the remaining pollen are classified as xerophytic (Mueller et al., 2016a, 2016b). Compared with AZ-I and AZ-III, hygrophytic plants increased in AZ-II, indicating an intensification of humid climatic conditions (Fig. 2).

In order to further constrain the trend of climatic conditions change in the target strata, we used CANOCO software to conduct a PCA based on the spore-pollen data. Results of PCA analysis are shown in Figs. 2, 3a, and 4. Two main ordination axes representing the largest variance in palynological composition are used to explain the two most dominant environmental gradients that control the dataset (e.g., Li et al., 2020; Zhang et al., 2022a). In this study, axis 1 and axis 2 separately account for 45.84 and 18.59 % of the sporomorph spectra difference, suggesting that axis 1 exerts the principal control on the dataset (Fig. 3a). On the positive side of axis 1, the hygrophytic spores (e.g., *Cyclogranisporites, Osmundacidites, Punctatisporites, Kraeuselisporites*, and *Triquitrites*) have high scores, and the xerophytic pollen (e.g., *Pseudopicea, Paleoconiferus*, and *Protoconiferus*) show high scores on the negative side of axis 1. Thus,

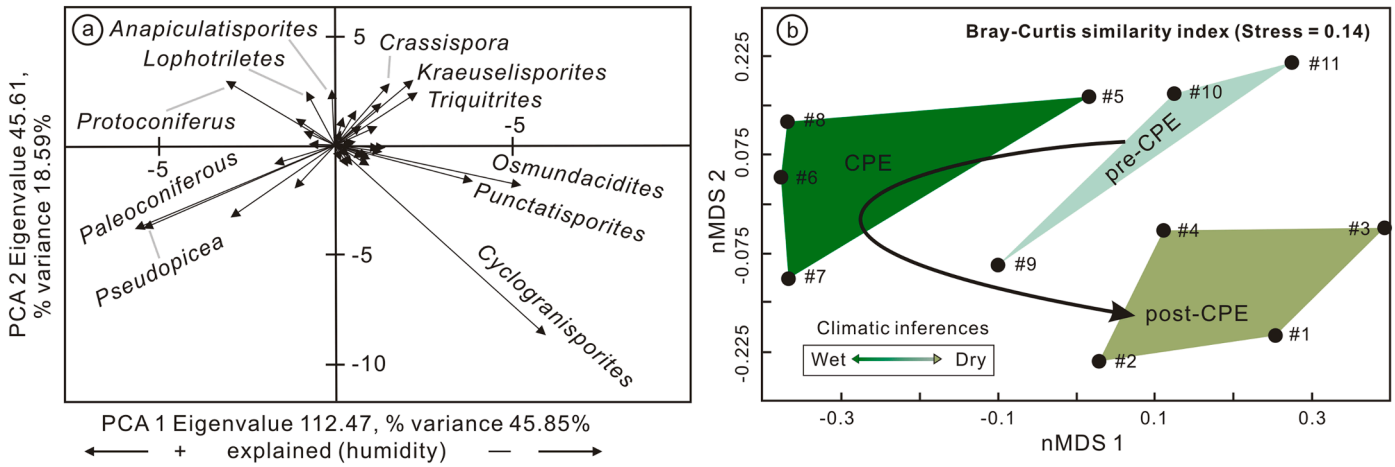

Fig. 3. Principal component analysis (PCA) (a) and non-metric multidimensional scaling (nMDs) (b) ordination plot of spore-pollen data from studied ZJ-1 borehole in the Jiyuan Basin.

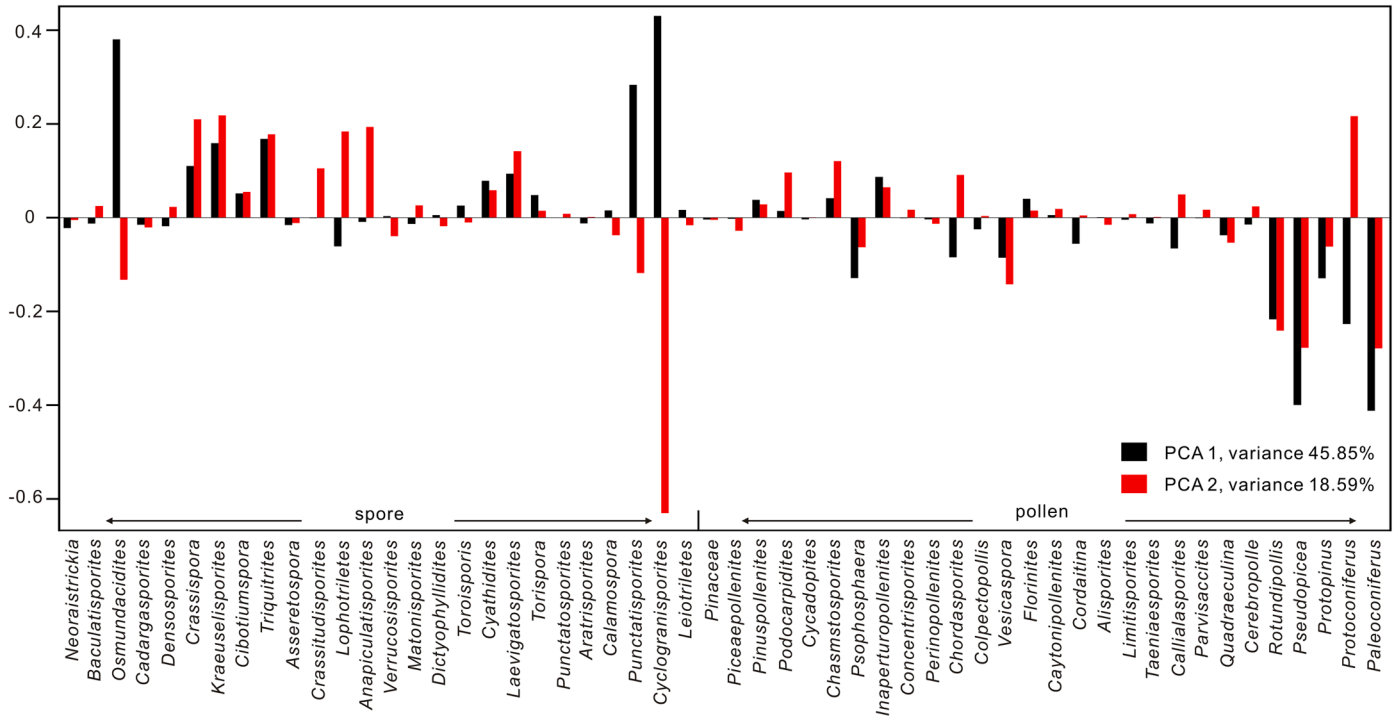

Fig. 4. Loading plots of PCA1 and PCA2 for spore-pollen genera from the studied ZJ-1 borehole in the Jiyuan Basin.

the first component axis is interpreted to reflect the changes in relative humidity (Fig. 3a). On the positive side of axis 2, fern spores (e.g., *Kraeuselisporites, Triquitrites, Anapiculatisporites, Lophotriletes*, and *Crassispora*) and conifer pollen *Protoconiferus* have high scores, and fern spores (e.g., *Cyclogranisporites, Osmundacidites*, and *Punctatisporites*) and conifer pollen *Pseudopicea* and *Paleoconiferus* show high scores on the negative side of axis 2 (Fig. 3a). Location of forms in relation to the second component axis is less clear and seems to be controlled by environment (e.g., Baranyi et al., 2019b; Fijałkowska-Mader et al., 2021). Although the second component can be associated with other palaeoclimatic variables such as temperature (e.g., Scott et al., 2012; Zhang et al., 2023b), lack of palaeotemperature proxies prevent us testing this hypothesis in our dataset.

The hygrophytic/xerophytic (H/X) ratio can provide further information on paleoclimate change (e.g., Zhang et al., 2023b, 2023c). The H/X ratio is a first-order approximation of a humidity signal, unless any of the exceptions mentioned occur in high abundance (Mueller et al., 2016a, 2016b). In the study area, H/X varies from 0.57 to 5.81 ($\bar{x}$ = 2.05) and increased in the CPE interval, indicating that increase of humid climatic conditions in this stage (Fig. 2).

Results of nMDs analysis based on the relative abundance of spore-pollen genera are shown in Fig. 3b. In this study, as shown in the discrete areas in ordination space of the nMDS plot (Fig. 3b), the distribution of palynological fossils is consistent with relatively arid climatic conditions in AZ-I and AZ-III, and relatively humid climatic conditions in AZ-II (inferred from the palynological abundance, PCA value, and H/X ratio changes). Furthermore, palynological fossils record obvious floral changes pre- and post-CPE on the nMDS plot (Fig. 3b). These samples plot a distance from the CPE samples (Fig. 3b), indicating a different plant taxonomic composition.

In summary, in AZ-II, the abundance of hygrophytes plants (including all spores and cycad pollen), the ratio of H/X, and the results

of PCA1 and nMDS significantly increased, indicating a dramatic increase in relative humid climatic conditions in the studied Jiyuan Basin during the CPE interval.

5. Discussion

5.1. Continental chemical weathering trends

Four episodes of increased CIA* values that exceed the background levels are accompanied by increases in kaolinite content in our lacustrine succession (Fig. 2). This suggests that four distinct episodes of enhanced continental chemical weathering occurred during the CPE. Because chemical weathering intensity is highly sensitive to paleoclimatic changes in temperature and precipitation in terrestrial settings (Zhang et al., 2019, 2023a; Yang et al., 2022; Xu et al., 2023) it is straightforward to invoke a climatic driver for the enhanced CIA* and kaolinite input but at the same time, weathering rates can also be affected by changes in provenance, depositional recycling, hydraulic or sedimentary sorting, and diagenesis (Chen et al., 2003; Lu et al., 2020; Yang et al., 2022; Zhang et al., 2022b). The potential impacts of these latter factors on the weathering proxies need to be excluded first in order to make any meaningful inferences about past temperature and humidity conditions.

The CIA* values have a significant positive correlation with CIA (r^2= 0.98) (Fig. 5a), suggesting that this correction eliminated the effects of K-metasomatism on CIA values without changing their temporal trends (Yang et al., 2022). All samples are distributed along the ideal weathering trend line of the upper crust in the southern NCP on the CIA (CIA*) -WIP (WIP*) diagram (Fig. S1b). This suggests that the provenance of the southern NCP experienced a continuous and consistent supply and that samples are not affected by changes in provenance or sedimentary recycling (Yang et al., 2022), in line with previous conclusions that Late Triassic sediments of the Jiyuan Basin were mainly sourced from the southern NCP (Yang et al., 2012). The Th/U ratios vary between 1.24 and 5.37 (Table S1) in the study area, indicating that samples are not affected by depositional recycling. This is because recycled mudstone sediments generally have Th/U ratios greater than six due to oxidation of U^{4+} to U^{6+} and its removal as a soluble component (c.f. Bhatia and Taylor, 1981; Lu et al., 2020).

Mudstone samples show poor correlation between Al_2O_3/SiO_2 ratio and CIA* values (Fig. 5b), WIP* values (Fig. 5c), and τNa values (Fig. 5d), suggesting that samples have not been significantly affected by hydraulic or sedimentary sorting processes or changes in grain size (Yang et al., 2022; Zhang et al., 2022b). High KI values (>0.25Δ°/2θ) and its random distributions vertically through the sedimentary succession (Fig. 2, Table S3), as well as the low organic matter maturity (Lu et al., 2021), indicate that samples from our studied site have not been diagenetically altered either (Zhang et al., 2021, 2022b). Furthermore, authigenic clay minerals can influence the clay mineral analysis of paleoclimate changes (e.g., Zhang et al., 2022b). Previous studies on

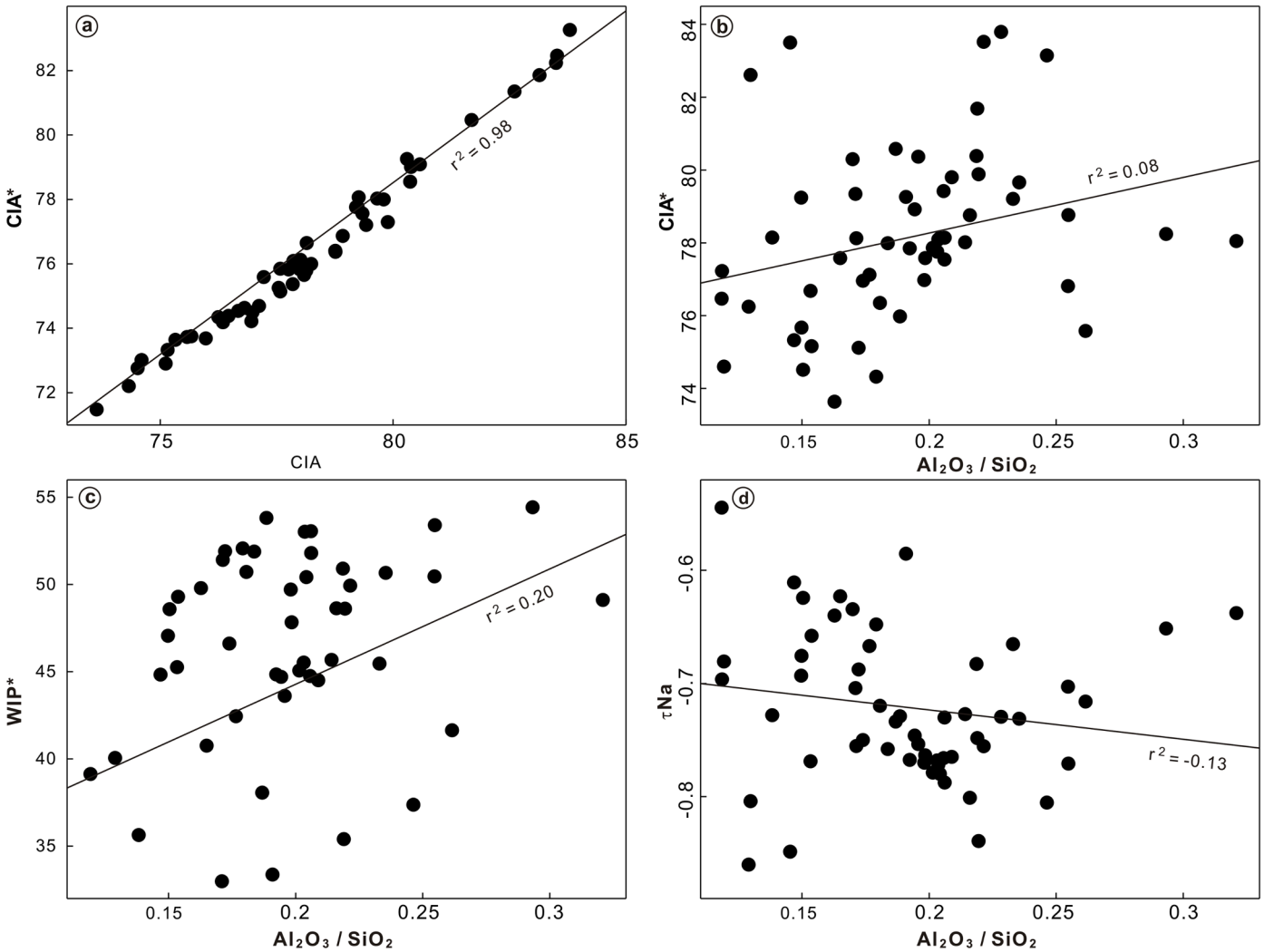

Fig. 5. Plots of CIA vs CIA* (a), Al_2O_3/SiO_2 ratio vs CIA* (b), WIP (c), and K/Si (d) from the ZJ-1 borehole in the Jiyuan Basin.

clay mineral origins in modern basins have shown that clay minerals in rivers and lakes have similar detrital characteristics to those in their surrounding basins (Court et al., 1972; Tomadin et al., 1986; Chamley, 1989). In freshwater rivers and lakes, an absence of cations and silicon limits in-situ formation of authigenic clay minerals (Gao et al., 2013; Gao, 2017). For these reasons, we assume that fewer authigenic clay minerals may be present in the research area. Therefore, we infer that clay minerals in the Jiyuan lake basin were mainly of detrital origin and were barely affected by diagenesis and authigenesis.

In summary, changes in the CIA* and kaolinite content in this study are considered to be reliable indicators of continental chemical weathering and paleoclimate dynamics. The evidence suggests that the clay minerals in the Jiyuan lake basin represent the product of intense chemical weathering driven by four episodes of dramatic climatic changes, rather than by local changes in sedimentary dynamics or diagenesis. While the maximum values in CIA do not greatly exceed the background CIA* values of 78 in the study area, the recorded CIA* peaks (84) show remarkable temporal correlation with CIEs and Hg peaks and suggest a true indication of four periods of enhanced weathering (Fig. 2). More general analysis of CIA* and kaolinite in the Jiyuan lake basin prior, during, and after the CPE demonstrates an increase in chemical weathering intensity across the CPE during which kaolinite almost doubled in content (Fig. 6). That kaolinite content does not seem to return entirely to pre-CPE values could point to sustained enhanced weathering well after the pluvial episode and potentially a delayed climatic recovery (Fig. 2).

5.2. CPE-related paleoclimate changes

Relatively warm and humid climatic conditions that promote continental chemical weathering appear to have prevailed globally during the CPE interval (Sun et al., 2016; Baranyi et al., 2019a; Dal Corso et al., 2020; Zhang et al., 2023c). The study area marks peaks of chemical weathering during the CPE interval (Figs. 2, 7) and each is accompanied by a simultaneous increase in the abundance of hygrophyte plants, H/X ratio, and changes in PCA and nMDs analysis results (Figs. 2, 3, 4) that are indicative of concurrent wetter climatic conditions (Lu et al., 2021). Consistent with previous studies of the chemical weathering index αi_{Al}, kaolinite content, and hygrophyte plant composition in the northwestern Tethys (Hungary) (Rostási et al., 2011; Baranyi et al., 2019a, 2019b), there is a clear link between enhanced continental chemical weathering and more humid conditions during the CPE. What stands out is that our high-resolution record reveals that enhanced weathering occurred in four distinct episodes alongside the rise in hygrophyte plant abundance (Fig. 2). In addition, marine strata in the Western Tethys contain four intervals of increased terrigenous sediment supply during the CPE which were explained by periodically increased terrestrial runoff and weathering caused by humid climatic pulses (Hornung and Brandner, 2005; Dal Corso et al., 2015, 2018). The introduction of terrigenous material into the oceans through enhanced terrestrial weathering may have contributed to the disappearance of marine life (Dal Corso et al., 2015, 2020), similar to what is believed to have occurred during the Permian-Triassic (Algeo et al., 2011; Lu et al., 2020; Frank et al., 2021; Xu et al., 2023; Zhang et al., 2023d) and the Triassic-Jurassic mass extinctions (Shen et al., 2022; Zhang et al., 2023d).

Oxygen isotope records from the Northern Calcareous Alps (Hornung et al., 2007a), the Lagonegro Basin (Trotter et al., 2015), and the Nanpanjiang Basin (South China) (Sun et al., 2016) show that the temperature increased by about 4℃ at the beginning of CPE, and a long-term warming trend of about 7℃ occurred later in the CPE. In this study (Figs. 2, 7) and others (Baranyi et al., 2019a; Pecorari et al., 2023), multiple periods of enhanced continental chemical weathering during the CPE were accompanied by CIEs, suggesting that global warming caused by the massive release of isotopically light CO_2 promoted continental chemical weathering. In our study, we find synchronous increases in weathering proxies, kaolinite, Hg peaks and CIEs (Fig. 2), while in the Western Tethys a kaolinite rise is delayed after the NCIEs. This variation in timing may be explained by the distance between the terrestrial kaolinite source and the marine depositional setting (Pecorari et al., 2023), with the Jiyuan lacustrine basin is likely closer to the source of kaolinite. The rapid (synchronous) response in kaolinite peaks after volcanism in our study area may also have been related to it having a more humid climate than the Western Tethys. Palynological evidence that show pre-CPE western Tethys Ocean was dominated by relatively arid climatic conditions (Roghi, 2004; Roghi et al., 2010; Dal Corso et al., 2020) while the NCP experienced relatively humid conditions since the Ladinian Stage (Jin et al., 2021). This conclusion is further be supported by general circulation model simulations (Sellwood and Valdes, 2006) showing that the western Tethys was drier and experienced less rainfall than the eastern Tethys (including the NCP) during the Late Triassic.

The regional surface temperature change can be estimated based on the relationship between the CIA and land surface temperatures during the Carnian Stage as identified in previous studies (Zhang et al., 2021). This approach has also been applied in different geological time intervals (Li and Yang, 2010; Frank et al., 2021; Zhang et al., 2021; Yang et al., 2022). The Carnian temperature-CIA relationship predicts that

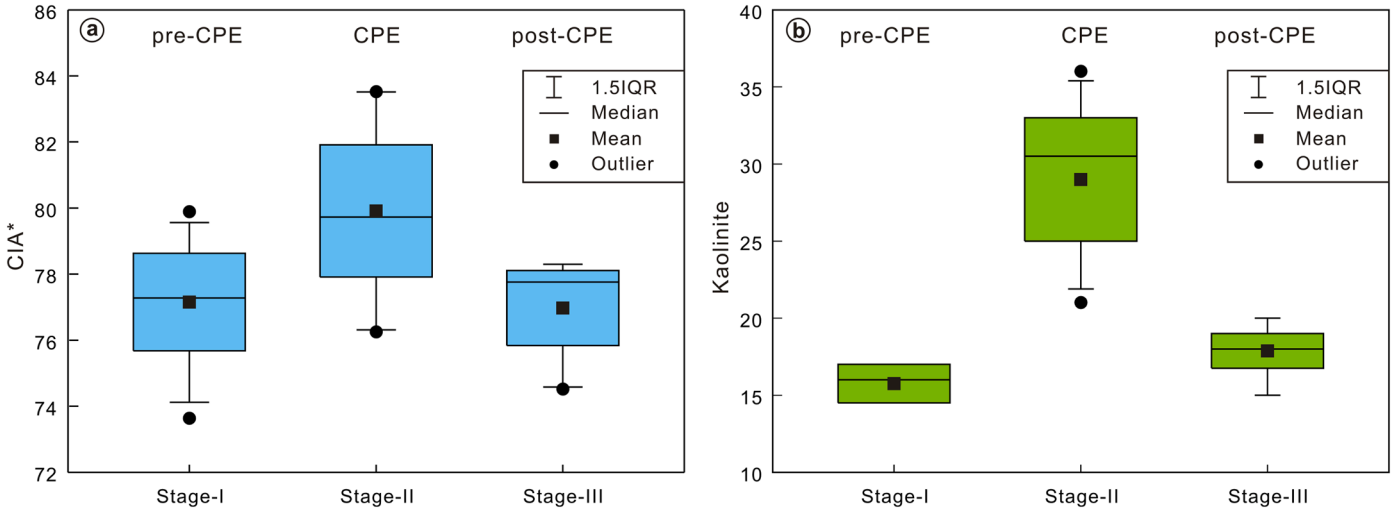

Fig. 6. Boxplot of CIA* values and kaolinite contents from the studied ZJ-1 borehole in the Jiyuan Basin.

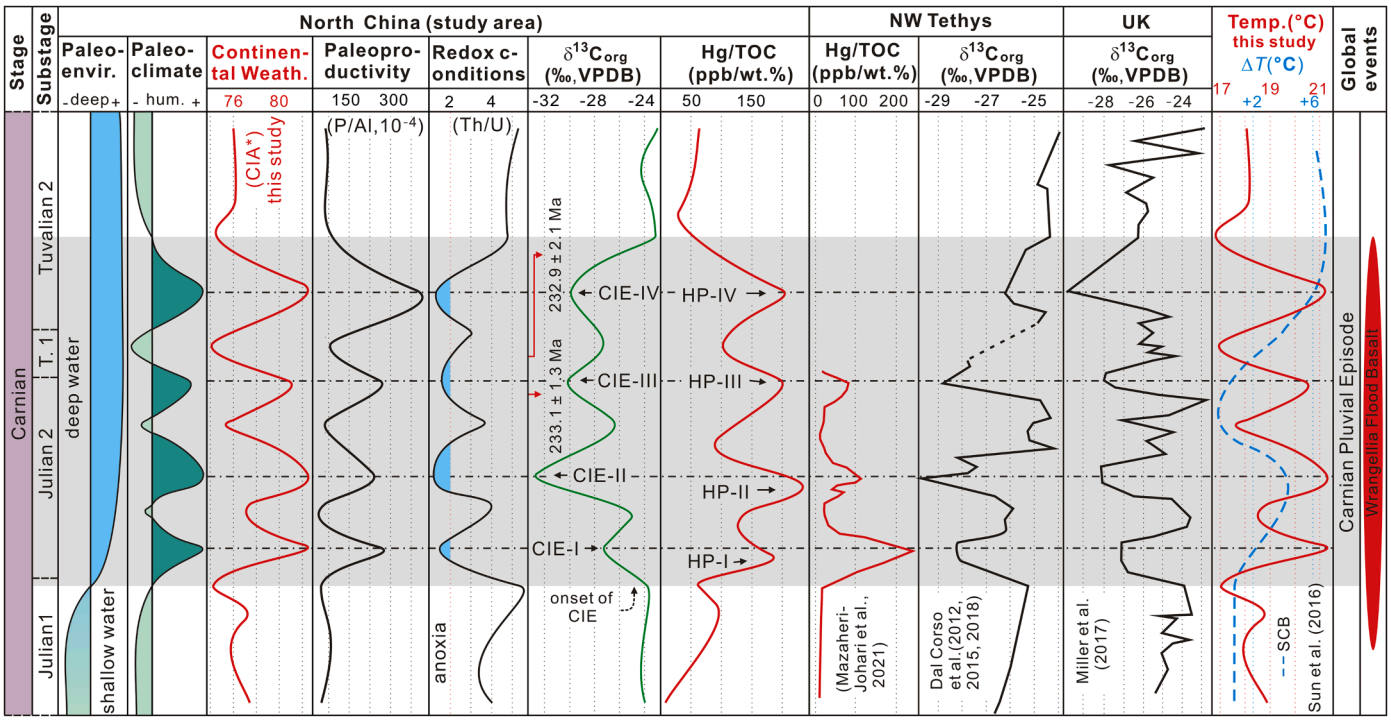

Fig. 7. Correlations of paleoenvironment, paleoclimate, continental weathering, paleoproductivity, redox conditions, $\delta^{13}C_{org}$ values, Hg/TOC ratios, temperature, and global events from Julian 1 to Tuvalian 2 Substages during the Late Triassic Carnian Stage. The stratigraphic framework is from (Dal Corso et al., 2020; Lu et al., 2021). Note that the palaeoclimate curves are obtained from a combined analysis of CIA values, kaolinite content, hygrophytic plants abundance, H/X ratio, PCA1 values, and nMDS. Abbreviations: T. 1 = Tuvalian 1; Paleoenv. = paleoenvironment; hum. = humidity; Weath. = Weathering; CIE-I to CIE-IV = organic CIEs I to IV; HP-I to HP-IV = Hg/TOC peak I to IV; VPDB = Vienna Pee Dee Belemnite; NW = Northwest; UK = United Kingdom; Tem. = Temperature; SCB = South China Block.

regional annual mean temperatures rose temporarily about 3.1 to 4.1 °C during the four distinct episodes (Figs. 2, 7, and Table S2), from ~16 °C to ~21 °C. These baseline temperatures are broadly consistent with general circulation models (GCM) that simulate the Late Triassic Climate (Sellwood and Valdes, 2006). In this GCM, the approximate Jiyuan Basin region experiences a winter season mean temperature between 0 and 4℃, and a summer season mean temperature between 36 and 40℃ (Sellwood and Valdes, 2006); from this we would expect the annual mean temperature in the Jiyuan Basin around 20℃, in agreement with the reconstructed mean annual temperature calculated using CIA. While it is challenging to distinguish temperature from humidity effects on chemical weathering, these estimates are in general agreement with the oxygen isotope temperatures throughout the CPE (Hornung et al., 2007a; Trotter et al., 2015; Sun et al., 2016). We propose that the study area experienced four geologically rapid and relatively warm-humid climatic pulses during the CPE, each of which temporarily promoted continental chemical weathering.

5.3. Causal link with Wrangellia volcanism

Four CIA* and kaolinite peaks occur almost simultaneously with reduced $\delta^{13}C_{org}$ values and elevated Hg concentrations (Hg/TOC ratio) in the Jiyuan Basin (Fig. 2). In a previous study (Lu et al., 2021), we ruled out that the negative CIEs in borehole ZJ-1 are the result of diagenetic processes and provided evidence for the volcanic origin of the negative CIEs and peaks in Hg, as opposed to a terrestrial origin driven by enhanced runoff of organic-rich sediments. Hg cycling in the terrestrial realm is complicated (Shen et al., 2019, 2020). In addition to volcanism, enhanced chemical weathering can accelerate Hg accumulation in catchment areas. The relatively warm and humid climatic conditions during the CPE could be inducive to this process and thereby affect the magnitude of the Hg peak. However, the sediments in the study area during the CPE interval were mainly derived from the northern QDOB and the southern NCP, transporting mainly gneiss, amphibolite, tonalite, trondhjemite, and granodiorite minerals with almost no organic matter (e.g., Dong and Santosh, 2016). This rules out the enhanced weathering leading to the increase of mercury concentration associated with the organic matter in the source area. Furthermore, the decrease in the C/N ratio and the increase in the algae/spore-pollen ratio and sapropelinite proportion during the CPE indicates higher contributions of aquatic organic matter to the lake, rather than enhanced terrestrial input of organic matter that would produce Hg peaks of non-volcanic origin (Fig. 2; Lu et al., 2021).

Multiple Hg enrichments during the CPE have been recorded from North China (this study area), South China (Zhao et al., 2022), Panthalassa (Japan) (Jin et al., 2023), and the western Tethys (Mazaheri-Johari et al., 2021) (Figs. 7, S3), suggesting that they represent a consistent, globally signal. The Hg isotopic composition from South China (Zhao et al., 2022) and Panthalassa (Japan) (Jin et al., 2023) (Fig. S3) indicate that the eruption of the Wrangellia LIP is the main cause of the global Hg enrichment anomaly during the CPE. In summary, we consider that the Hg peaks in the studied area are primarily related to Wrangellia volcanism and that the negative CIEs are global anomalies that have also been recorded in other lacustrine (Miller et al., 2017; Baranyi et al., 2019b) and marine records (Dal Corso et al., 2015, 2018; Sun et al., 2016; Tomimatsu et al., 2021) (Figs. 7, S3). The covariation relationship among CIA* and kaolinite peaks, CIEs and Hg/TOC ratio provides strong support for a link between Wrangallia LIP volcanism and chemical weathering rates (Figs. 2, 7). Further evidence that reinforces this link comes from the simultaneous decrease in $\delta^{13}C_{org}$ with each volcanic pulse that releases isotopically light carbon into the atmosphere-ocean system.

During the active eruption period of the Wrangellia LIP (inferred from the peaks of Hg concentration and Hg/TOC ratio), massive

amounts of Hg and isotopically light CO_2 entered the atmospheric system, causing a strong greenhouse effect and promoting global warming, producing negative CIEs, and Hg concentration (Hg/TOC ratio) enrichment (Dal Corso et al., 2015, 2018; Miller et al., 2017; Lu et al., 2021; Mazaheri-Johari et al., 2021) (Figs. 2, 7, 8). In response to global warming, increased evapotranspiration and greater land-ocean temperature contrast likely led to a more intense atmospheric circulation and hydrological cycle (Dal Corso et al., 2020). Rainfall increased (inferred from increases in hygrophytes plants and lake area expansion and deepening) (Lu et al., 2021) and climate generally became more humid in the study area (inferred from increase in hygrophytes plants, CIA values and kaolinite content, H/X ratio, and PCA and nMDS analysis) (Figs. 2, 3, 7, 8). The initial global warming could have been further amplified by positive feedbacks such as the accelerated bacterial and fungal decomposition of organic matter that release carbon stored in soils back into the atmosphere (Brady, 1991).

Warm-humid conditions promoted continental chemical weathering (inferred from the increase of CIA* value and kaolinite content) in the study area (Figs. 2, 7, 8). In combination with increased terrestrial runoff (inferred from the increase of P/Al ratio (Lu et al., 2021)), this would have enhanced the nutrient flux into the lake and thereby drive an increase in lake primary productivity and algal blooms (Figs. 7, 8). Extreme productivity in turn develops dysoxic-anoxic conditions (inferred from the decrease of Th/U ratio), enhances the preservation of organic carbon (inferred from the increase of TOC values (Lu et al., 2021)), and drives the loss of aquatic organisms (inferred from the disappearance of animal fossils) (Lu et al., 2021) (Figs. 7, 8). Rising surface temperatures (Figs. 2, 7, 8) may have further promoted algae blooms (inferred from the changes in C:N ratio, the algae/spore-pollen ratio, and the sapropelinite proportion; Lu et al., 2021) in the Jiyuan Basin lake. In modern ecosystems, the optimal growth temperature for both chlorophytes and harmful cyanobacteria in freshwater environments is about 20–32℃ (Paerl and Otten, 2013; Lürling et al., 2018), which is consistent with the estimated surface temperature during CPE in the study area (Figs. 2, 7, and Table S2). The enhanced remineralization that results from algal blooms also reduces the dissolved oxygen concentrations in these intermittent waterbodies and likely produced secondary metabolites toxic to animals (e.g., Paerl and Otten, 2013; Zhang et al., 2022a), which may have contributed to an anoxic environment in the Jiyuan lake and led to the extinction of aerobic organisms.

Our proxies indicate the reverse chain of reactions in the waning stages of the Wrangellia LIP (inferred from the decline in Hg concentration and Hg/TOC ratio). Reduced volcanic outgassing, enhanced continental weathering, and burial of organic carbon would have lowered atmospheric CO_2 and led to the subsequent recovery of $\delta^{13}C_{org}$ after the negative excursions (Figs. 2, 7, 8). Decreased atmospheric CO_2 concentrations and surface temperatures weaken the global hydrological cycle, reduce the lake nutrient input (inferred from the decrease in P/Al ratio and Th/U ratio), productivity, and ultimately reduce the burial of organic carbon (Lu et al., 2021) (Figs. 2, 7, 8). Lower CO_2 concentrations and temperatures in turn weaken continental weathering (inferred from declines in CIA* values and kaolinite content) (Figs. 2, 7, 8), as also observed during the end-Triassic mass extinction (Shen et al., 2022).

What makes this lake record particularly interesting are the four distinct peaks with remarkable correlation between the volcanic input, continental weathering, and $\delta^{13}C_{org}$ at high resolution (Figs. 2, 7, 8). The

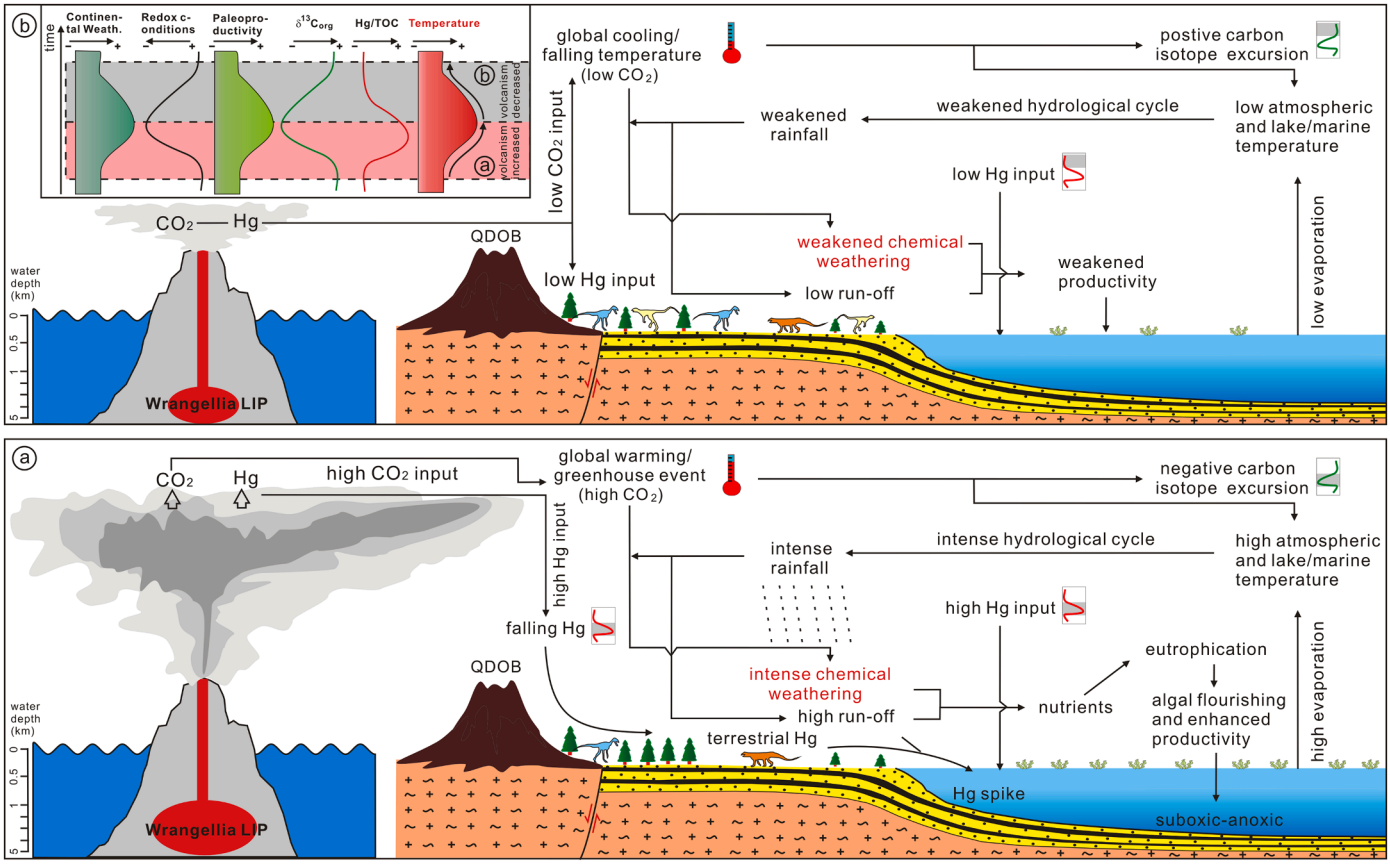

Fig. 8. Schematic reconstructions examining how the Wrangellia Large Igneous Province (LIP) might have driven climatic and environmental changes in North China during the Late Triassic Carnian Stage. (a) Onset of LIP volcanism with increasing surface temperature, continental weathering rates and paleoproductivity. (b) Decline of LIP volcanism with decreasing surface temperature, continental weathering rates and paleoproductivity. Abbreviations: weath. = weathering; QDOB = Qingling-Dabie Orogenic Belt.

Hg/TOC ratio shows that isotopically light volcanic outgassing of carbon occurred in four major pulses with a near instantaneous impact on $\delta^{13}C_{org}$, repeatedly reducing values by about 4‰ over periods less than 2 Ma in duration. A small (1–2 meter) temporal offset between Hg-I/Hg-II and CIE-I/CIE-II results from the different pathways by which Hg and carbon isotopes travel though the system. Hg particles settle at the surface in less than two years after their volcanic release (Schroeder and Munthe, 1998), whereas carbon isotopes have a much longer residence time. Because of slow incorporation into organic matter and low settling rates, it takes several thousands of years for the excursion to be fully expressed in the geological record. Such temporal Hg-$\delta^{13}C$ offsets have also been observed for the Palaeocene-Eocene Thermal Maximum (Jones et al., 2019; Jin et al., 2023) and the Permian-Triassic mass extinction (Shen et al., 2019).

The largest negative excursion recorded here is 'CIE-II' with $\delta^{13}C_{org}$ reduced by 7‰ (Fig. 2). Other $\delta^{13}C$ records from marine marginal (Dal Corso et al., 2015, 2018; Li et al., 2022), deep marine (Sun et al., 2016; Tomimatsu et al., 2021), and lacustrine (Miller et al., 2017; Baranyi et al., 2019b; Lu et al., 2021) settings also record multiple CIEs (Dal Corso et al., 2018, 2020) which implies their global nature, although the number of CIEs and their magnitudes vary due to environmental and depositional differences, and/or sampling resolution. While these factors can obscure CIEs, they cannot amplify negative CIEs with a constant terrestrial:marine carbon source ratio, hence the four CIEs are a true feature. More than 30,000 Pg of volcanic carbon with a canonical isotope signature of −6‰ is required to produce CIEs of this magnitude (Vervoort et al., 2019). This is considered a lower estimate because the Carnian total exogenic carbon pool was likely much larger than that used in Vervoort et al. (2019); i.e. much more carbon input was required during the Carnian than during the Cenozoic to produce a similar excursion.

The seemingly rapid recoveries to pre-CIE $\delta^{13}C_{org}$ values are particularly striking and can be explained by 1) enhanced weathering delivering isotopically heavy carbon to the atmosphere-ocean system, and 2) increased removal or burial of isotopically light carbon. While the isotopic impact of weathered carbon may be small because the isotopic signature of weathered carbonate rocks is only slightly heavier than that of the atmosphere and ocean, the impact may have been amplified in the Carnian in absence of abundant pelagic calcifiers prior to the CPE (Preto et al., 2014; Dal Corso et al., 2021) that prevent deep marine carbonate compensation (Ridgwell, 2005; Goddéris et al., 2008) and subsequent removal of isotopically heavy carbon. Enhanced organic carbon burial is expected to have had the greatest influence on CIE recovery to more positive values and it is important to emphasize both the speed and magnitude at which excess organic carbon burial must have occurred. The occurrence of widespread dysoxic and anoxic conditions in both marine (Sun et al., 2016; Tomimatsu et al., 2021) and lacustrine environments (Lu et al., 2021) likely played a crucial role in promoting organic carbon burial on a global scale.

6. Conclusions

(1) In the Jiyuan Basin, the CPE includes four short-duration, high intensity pulses of enhanced continental weathering identified by peaks in CIA* values and kaolinite content. Geochemical and mineralogical analyses show that the CIA* values and kaolinite contents are reliable proxies for temperature and humidity paleoclimatic conditions, and are not affected by changes in provenance, sedimentary recycling, hydraulic sorting, or diagenesis.

(2) The four pulses of elevated CIA* values and kaolinite content roughly correspond with significant increases in the abundance of terrestrial hygrophytic plants, negative carbon isotope excursions, and peaks in Hg concentration (Hg/TOC ratio). Collectively these indicate that short, intense pulses of volcanism drove warm and humid conditions in the Jiyuan Basin.

(3) A possible relationship between climatic perturbations leading to enhanced chemical weathering and the Wrangellia LIP during the CPE is suggested. Each pulse of Wrangellia volcanism released large amounts of isotopically light CO_2 and Hg into the atmosphere-ocean system, and drove short but intense episodes of global warming. In turn, the global hydrological cycle intensified and significantly increased rates of continental chemical weathering. Enhanced continental weathering resulted in increased nutrient fluxes into the Jiyuan Basin lake through terrestrial runoff, which led to eutrophication, higher productivity, and anoxic water conditions in the lake ecosystem that promoted the burial of organic matter. Conversely, the sustained enhanced continental weathering and organic carbon burial reduced atmospheric CO_2 concentrations rapidly following each volcanic pulse, lowered surface temperatures and weakened the hydrological cycle weakening so that continental weathering and organic carbon burial rates returned to their initial fluxes prior to the volcanic perturbation.

CRediT authorship contribution statement

Peixin Zhang: Writing – review & editing, Writing – original draft, Methodology, Investigation, Formal analysis, Data curation. **Minfang Yang:** Writing – review & editing, Writing – original draft, Supervision, Project administration, Methodology, Funding acquisition, Formal analysis, Conceptualization. **Jing Lu:** Writing – review & editing, Writing – original draft, Visualization, Validation, Supervision, Resources, Project administration, Methodology, Investigation, Funding acquisition, Formal analysis, Conceptualization. **Zhongfeng Jiang:** Writing – review & editing. **Pam Vervoort:** Writing – review & editing, Writing – original draft, Investigation. **Kai Zhou:** Writing – review & editing, Investigation. **Xiaotao Xu:** Writing – review & editing, Investigation. **Huijuan Chen:** Writing – review & editing. **Ye Wang:** Methodology, Investigation, Conceptualization. **Zhen He:** Writing – review & editing, Investigation. **Xiao Bian:** Investigation, Writing – review & editing. **Longyi Shao:** Writing – review & editing, Validation, Supervision, Project administration, Funding acquisition, Conceptualization. **Jason Hilton:** Writing – review & editing, Writing – original draft, Visualization, Validation, Supervision, Resources, Project administration, Methodology, Investigation, Formal analysis, Conceptualization.

Declaration of Competing Interest

The authors declare that they have no known competing financial interests or personal relationships that could have appeared to influence the work reported in this paper.

Data availability

The core is housed at the State Key Laboratory of Coal Resources and Safe Mining (Beijing). All data needed to evaluate the conclusions are present in the paper and/or the *SI Appendix*.

Acknowledgements

We are grateful to Suping Peng and Shifeng Dai (China University of Mining and Technology Beijing) and Sarah E. Greene (University of Birmingham) for their comments on earlier versions of the manuscript. We also thank Andrew Jacobson and two anonymous reviewers for constructive and helpful reviews and comments on the manuscript. Financial support was provided by the National Key Research and Development Program of China (2022YFF0800203/01), the National Natural Science Foundation of China (Grant nos. 42172196, 41772161, and 41472131), the Fund of Henan University of Urban Construction (K-Q2023019), and the Natural Environment Research Council (UK) award

NE/W009625/1.

Supplementary materials

Supplementary material associated with this article can be found, in the online version, at doi:10.1016/j.epsl.2023.118517.

References

Algeo, T.J., Kuwahara, K., Sano, H., Bates, S., Lyons, T., Elswick, E., Hinnov, L., Ellwood, B., Moser, J., Maynard, J.B., 2011. Spatial variation in sediment fluxes, redox conditions, and productivity in the Permian-Triassic Panthalassic Ocean. Palaeogeogr. Palaeoclimatol. Palaeoecol. 308, 65–83. https://doi.org/10.1016/j.palaeo.2010.07.007.

Baranyi, V., Miller, C.S., Ruffell, A., Hounslow, M.W., Kürschner, W.M., 2019a. A continental record of the carnian pluvial episode (CPE) from the Mercia mudstone group (UK): palynology and climatic implications. J. Geol. Soc. London 176, 149–166. https://doi.org/10.1144/jgs2017-150.

Baranyi, V., Rostási, Á., Raucsik, B., Kürschner, W.M., 2019b. Palynology and weathering proxies reveal climatic fluctuations during the Carnian Pluvial Episode (CPE) (Late Triassic) from marine successions in the Transdanubian Range (western Hungary). Glob. Planet Change 177, 157–172. https://doi.org/10.1016/j.gloplacha.2019.01.018.

Bhatia, M.R., Taylor, S.R., 1981. Trace-element geochemistry and sedimentary provinces: a study from the Tasman Geosyncline, Australia. Chem. Geol. 33, 115–125. https://doi.org/10.1016/0009-2541(81)90089-9.

Brady, P.V., 1991. The effect of silicate weathering on global temperature and atmospheric CO_2. J. Geophys. Res. 96, 18101. https://doi.org/10.1029/91JB01898.

Chamley, H., 1989. Clay Sedimentology Berlin. Springer-Verlag, Heidelberg.

Chen, T., Wang, H., Zhang, Z., Wang, H.J., 2003. Clay minerals as indicators of paleoclimate. Acta Petrol. Mineral 22, 416–505. https://doi.org/10.3969/j.issn.1000-6524.2003.z1.022.

Court, J.E., Goldman, C.R., Hyne, N.J., 1972. Surface sediments in Lake Tahoe, California–Nevada. J. Sediment. Res. 42 (2), 359–377.

Dal Corso, J., Bernardi, M., Sun, Y., Song, H., Seyfullah, L.J., Preto, N., Gianolla, P., Ruffell, A., Kustatscher, E., Roghi, G., Merico, A., Hohn, S., Schmidt, A.R., Marzoli, A., Newton, R.J., Wignall, P.B., Benton, M.J., 2020. Extinction and dawn of the modern world in the Carnian (Late Triassic). Sci. Adv. 6, eaba0099. https://doi.org/10.1126/sciadv.aba0099.

Dal Corso, J., Gianolla, P., Newton, R.J., Franceschi, M., Roghi, G., Caggiati, M., Raucsik, B., Budai, T., Haas, J., Preto, N., 2015. Carbon isotope records reveal synchronicity between carbon cycle perturbation and the "Carnian Pluvial Event" in the Tethys realm (Late Triassic). Glob. Planet Change 127, 79–90. https://doi.org/10.1016/j.gloplacha.2015.01.013.

Dal Corso, J., Gianolla, P., Rigo, M., Franceschi, M., Roghi, G., Mietto, P., Manfrin, S., Raucsik, B., Budai, T., Jenkyns, H.C., Reymond, C.E., Caggiati, M., Gattolin, G., Breda, A., Merico, A., Preto, N., 2018. Multiple negative carbon-isotope excursions during the Carnian Pluvial Episode (Late Triassic). Earth-Science Rev. 185, 732–750. https://doi.org/10.1016/j.earscirev.2018.07.004.

Dal Corso, J., Mietto, P., Newton, R.J., Pancost, R.D., Preto, N., Roghi, G., Wignall, P.B., 2012. Discovery of a major negative ^{13}C spike in the Carnian (Late Triassic) linked to the eruption of Wrangellia flood basalts. Geology 40, 79–82. https://doi.org/10.1130/G32473.1.

Dal Corso, J., Mills, B.J.W., Chu, D., Newton, R.J., Song, H., 2022. Background Earth system state amplified Carnian (Late Triassic) environmental changes. Earth Planet Sci. Lett. 578, 117321 https://doi.org/10.1016/j.epsl.2021.117321.

Dal Corso, J., Preto, N., Agnini, C., Hohn, S., Merico, A., Willems, H., Gianolla, P., 2021. Rise of calcispheres during the Carnian Pluvial Episode (Late Triassic). Glob. Planet. Change 200, 103453. https://doi.org/10.1016/j.gloplacha.2021.103453.

Dong, Y., Santosh, M., 2016. Tectonic architecture and multiple orogeny of the Qinling Orogenic Belt, Central China. Gondwana Res. 29, 1–40. https://doi.org/10.1016/j.gr.2015.06.009.

Fedo, C.M., Nesbitt, W.H., Young, G.M., 1995. Unraveling the effects of potassium metasomatism in sedimentary rocks and paleosols, with implications for paleoweathering conditions and provenance. Geology 23, 921. https://doi.org/10.1130/0091-7613(1995)023.0921:UTEOPM.2.3.CO;2.

Fijałkowska-Mader, A., Jewuła, K., Bodor, E., 2021. Record of the Carnian Pluvial Episode in the Polish microflora. Palaeoworld 30, 106–125. https://doi.org/10.1016/j.palwor.2020.03.006.

Frank, T.D., Fielding, C.R., Winguth, A.M.E., Savatic, K., Tevyaw, A., Winguth, C., McLoughlin, S., Vajda, V., Mays, C., Nicoll, R., Bocking, M., Crowley, J.L., 2021. Pace, magnitude, and nature of terrestrial climate change through the end-Permian extinction in southeastern Gondwana. Geology 49, 1089–1095. https://doi.org/10.1130/G48795.1.

Gao, S., Luo, T.C., Zhang, B.R., Zhang, H.F., Han, Y.W., Zhao, Z.D., Hu, Y.K., 1998. Chemical composition of the continental crust as revealed by studies in east China. Geochim. Cosmochim. Acta 62, 1959–1975. https://doi.org/10.1016/S0016-7037(98)00121-5.

Gao, X., 2017. Clay Mineralogy. Chemical Industry Press, Beijing.

Gao, Y., Wang, C., Liu, Z., Zhao, B., Zhang, X., 2013. Clay mineralogy of the middle Mingshui Formation (upper Campanian to lower Maastrichtian) from the SKIn borehole in the Songliao Basin, NE China: implications for palaeoclimate and provenance. Palaeogeogr. Palaeoclimatol. Palaeoecol. 385, 162–170. https://doi.org/10.1016/j.palaeo.2012.10.038.

Goddéris, Y., Donnadieu, Y., de Vargas, C., Pierrehumbert, R.T., Dromart, G., van de Schootbrugge, B., 2008. Causal or casual link between the rise of nannoplankton calcification and a tectonically-driven massive decrease in Late Triassic atmospheric CO_2? Earth Planet Sci. Lett. 267, 247–255. https://doi.org/10.1016/j.epsl.2007.11.051.

Hammer, Ø., Harper, D.A.T., Ryan, P.D., 2001. PAST : paleontological statistics software package for education and data analysis. Palaeontol. Electron. 4, 1–9.

Hornung, T., Brandner, R., 2005. Biochronostratigraphy of the Reingraben Turnover (Hallstatt Facies Belt): local black shale events controlled by regional tectonics, climatic change and plate tectonics. Facies 51, 460–479. https://doi.org/10.1007/s10347-005-0061-x.

Hornung, T., Brandner, R., Krystyn, L., Joachimski, M.M., Keim, L., 2007a. Multistratigraphic constraints on the NW Tethyan "Carnian crisis. New Mex. Museum Nat. Hist. Sci. Bull. 41, 59–67.

Hornung, Thomas, Krystyn, L., Brandner, R., 2007b. A Tethys-wide mid-Carnian (Upper Triassic) carbonate productivity crisis: evidence for the Alpine Reingraben Event from Spiti (Indian Himalaya)? J. Asian Earth Sci. 30, 285–302. https://doi.org/10.1016/j.jseaes.2006.10.001.

Huang, Y., Zhang, C., Zhu, R., Yi, X., Qu, J., Tang, Y., 2017. Palaeoclimatology, provenance and te0ctonic setting during late Permian to Middle Triassic in Mahu Sag, Junggar Basin, China. Earth Sci. 42, 1736–1749. https://doi.org/10.3799/dqkx.2017.559.

Jin, X., Baranyi, V., Caggiati, M., Franceschi, M., Wall, C.J., Liu, G., Schmitz, M.D., Gianolla, P., Ogg, J.G., Lu, G., Shi, Z., Preto, N., 2021. Middle Triassic lake deepening in the Ordos Basin of North China linked with global sea-level rise. Glob. Planet Change 207, 103670. https://doi.org/10.1016/j.gloplacha.2021.103670.

Jin, X., Gianolla, P., Shi, Z., Franceschi, M., Caggiati, M., Du, Y., Preto, N., 2020. Synchronized changes in shallow water carbonate production during the Carnian Pluvial Episode (Late Triassic) throughout Tethys. Glob. Planet Change 184, 103035. https://doi.org/10.1016/j.gloplacha.2019.103035.

Jin, S., Kemp, D.B., Yin, R., Sun, R., Shen, J., Jolley, D.W., Vieira, M., Huang, C., 2023. Mercury isotope evidence for protracted North Atlantic magmatism during the Paleocene-Eocene Thermal Maximum. Earth Planet. Sci. Lett. 602, 117926 https://doi.org/10.1016/j.epsl.2022.117926.

Jin, X., Tomimatsu, Y., Yin, R., Onoue, T., Franceschi, M., Grasby, S.E., Du, Y., Rigo, M., 2023. Climax in Wrangellia LIP activity coincident with major Middle Carnian (Late Triassic) climate and biotic changes: Mercury isotope evidence from the Panthalassa pelagic domain. Earth Planet. Sci. Lett. 607, 118075. https://doi.org/10.1016/j.epsl.2023.118075.

Jones, M.T., Percival, L.M.E., Stokke, E.W., Frieling, J., Mather, T.A., Riber, L., Schubert, B.A., Schultz, B., Tegner, C., Planke, S., Svensen, H.H., 2019. Mercury anomalies across the Palaeocene-Eocene Thermal Maximum. Clim. Past 15, 217–236. https://doi.org/10.5194/cp-15-217-2019.

Kozur, H.W., Bachmann, G.H., 2010. The Middle Carnian Wet Intermezzo of the Stuttgart Formation (Schilfsandstein), Germanic Basin. Palaeogeogr. Palaeoclimatol. Palaeoecol. 290, 107–119. https://doi.org/10.1016/j.palaeo.2009.11.004.

Lepš, J., Šmilauer, P., 2003. Multivariate Analysis of Ecological Data Using CANOCO. Cambridge University Press, Cambridge. https://doi.org/10.1017/CBO9780511615146.

Li, C., Yang, S., 2010. Is chemical index of alteration (CIA) a reliable proxy for chemical weathering in global drainage basins? Am. J. Sci. 310, 111–127. https://doi.org/10.2475/02.2010.03.

Li, L., Wang, Y., Kürschner, W.M., Ruhl, M., Vajda, V., 2020. Palaeovegetation and palaeoclimate changes across the Triassic – Jurassic transition in the Sichuan Basin, China. Palaeogeogr. Palaeoclimatol. Palaeoecol. 556, 109891 https://doi.org/10.1016/j.palaeo.2020.109891.

Li, Q., Ruhl, M., Wang, Y.D., Xie, X.P., An, P.C., Xu, Y.Y., 2022. Response of Carnian Pluvial Episode evidenced by organic carbon isotopic excursions from western Hubei, South China. Palaeoworld 31, 324–333. https://doi.org/10.1016/j.palwor.2021.08.004.

Liu, S., Su, S., Zhang, G., 2013. Early Mesozoic basin development in North China: indications of cratonic deformation. J. Asian Earth Sci. 62, 221–236. https://doi.org/10.1016/j.jseaes.2012.09.011.

Lu, J., Zhang, P., Yang, M., Shao, L., Hilton, J., 2020. Continental records of organic carbon isotopic composition ($\delta^{13}C_{org}$), weathering, paleoclimate and wildfire linked to the End-Permian Mass Extinction. Chem. Geol. 558, 119764 https://doi.org/10.1016/j.chemgeo.2020.119764.

Lu, J., Zhang, P., Dal Corso, J., Yang, M., Wignall, P.B., Greene, S.E., Shao, L., Lyu, D., Hilton, J., 2021. Volcanically driven lacustrine ecosystem changes during the Carnian Pluvial Episode (Late Triassic). Proc. Natl. Acad. Sci. USA 118, e2109895118. https://doi.org/10.1073/pnas.2109895118.

Lürling, M., Mello, M.M., van Oosterhout, F., de Senerpont Domis, L., Marinho, M.M., 2018. Response of natural cyanobacteria and algae assemblages to a nutrient pulse and elevated temperature. Front. Microbiol. 9, 1851. https://doi.org/10.3389/fmicb.2018.01851.

Mazaheri-Johari, M., Gianolla, P., Mather, T.A., Frieling, J., Chu, D., Dal Corso, J., 2021. Mercury deposition in Western Tethys during the Carnian Pluvial Episode (Late Triassic). Sci. Rep. 11, 17339. https://doi.org/10.1038/s41598-021-96890-8.

Miller, C.S., Peterse, F., da Silva, A.C., Baranyi, V., Reichart, G.J., Kürschner, W.M., 2017. Astronomical age constraints and extinction mechanisms of the Late Triassic Carnian crisis. Sci. Rep. 7, 2557. https://doi.org/10.1038/s41598-017-02817-7.

Mueller, S., Hounslow, M.W., Kürschner, W.M., 2016a. Integrated stratigraphy and palaeoclimate history of the Carnian Pluvial event in the Boreal realm; new data

from the Upper Triassic Kapp Toscana Group in central Spitsbergen (Norway). J. Geol. Soc. London 173, 186–202. https://doi.org/10.1144/jgs2015-028.
Mueller, S., Krystyn, L., Kürschner, W.M., 2016b. Climate variability during the Carnian pluvial phase — a quantitative palynological study of the Carnian sedimentary succession at Lunz am See, Northern Calcareous Alps, Austria. Palaeogeogr. Palaeoclimatol. Palaeoecol. 441, 198–211. https://doi.org/10.1016/j.palaeo.2015.06.008.
Nesbitt, H.W., Young, G.M., 1984. Prediction of some weathering trends of plutonic and volcanic rocks based on thermodynamic and kinetic considerations. Geochim. Cosmochim. Acta 48, 1523–1534. https://doi.org/10.1016/0016-7037(84)90408-3.
Paerl, H.W., Otten, T.G., 2013. Harmful cyanobacterial blooms: causes, consequences, and controls. Microb. Ecol. 65, 995–1010. https://doi.org/10.1007/s00248-012-0159-y.
Pecorari, M., Caggiati, M., Dal Corso, J., Cruciani, G., Tateo, F., Chu, D., Gianolla, P., 2023. Weathering and sea level control on siliciclastic deposition during the Carnian Pluvial Episode (Southern Alps, Italy). Palaeogeogr. Palaeoclimatol. Palaeoecol. 617, 111495 https://doi.org/10.1016/j.palaeo.2023.111495.
Preto, N., Willems, H., Guaiumi, C., Westphal, H., 2014. Erratum to: onset of significant pelagic carbonate accumulation after the Carnian Pluvial Event (CPE) in the western Tethys. Facies 60, 719–720. https://doi.org/10.1007/s10347-013-0387-8.
Ridgwell, A., 2005. A mid Mesozoic revolution in the regulation of ocean chemistry. Mar. Geol. 217, 339–357. https://doi.org/10.1016/j.margeo.2004.10.036.
Roghi, G., 2004. Palynological investigations in the Carnian of the Cave del Predil area (Julian Alps, NE Italy). Rev. Palaeobot. Palynol. 132, 1–35. https://doi.org/10.1016/j.revpalbo.2004.03.001.
Roghi, G., Gianolla, P., Minarelli, L., Pilati, C., Preto, N., 2010. Palynological correlation of Carnian humid pulses throughout western Tethys. Palaeogeogr. Palaeoclimatol. Palaeoecol. 290, 89–106. https://doi.org/10.1016/j.palaeo.2009.11.006.
Rostási, Á., Raucsik, B., Varga, A., 2011. Palaeoenvironmental controls on the clay mineralogy of Carnian sections from the Transdanubian Range (Hungary). Palaeogeogr. Palaeoclimatol. Palaeoecol. 300, 101–112. https://doi.org/10.1016/j.palaeo.2010.12.013.
Schroeder, W.H., Munthe, J., 1998. Atmospheric mercury—an overview. Atmos. Environ. 32, 809–822. https://doi.org/10.1016/S1352-2310(97)00293-8.
Scott, L., Neumann, F.H., Brook, G.A., Bousman, C.B., Norström, E., Metwally, A.A., 2012. Terrestrial fossil-pollen evidence of climate change during the last 26 thousand years in Southern Africa. Quat. Sci. Rev. 32, 100–118. https://doi.org/10.1016/j.quascirev.2011.11.010.
Sellwood, B.W., Valdes, P.J., 2006. Mesozoic climates: general circulation models and the rock record. Sediment. Geol. 190, 269–287. https://doi.org/10.1016/j.sedgeo.2006.05.013.
Shen, J., Yu, J., Chen, J., Algeo, T.J., Xu, G., Feng, Q., Shi, X., Planavsky, N.J., Shu, W., Xie, S., 2019. Mercury evidence of intense volcanic effects on land during the Permian-Triassic transition. Geology 47, 1117–1121. https://doi.org/10.1130/G46679.1.
Shen, J., Feng, Q., Algeo, T.J., Liu, Jinling, Zhou, C., Wei, W., Liu, Jiangsi, Them, T.R., Gill, B.C., Chen, J., 2020. Sedimentary host phases of mercury (Hg) and implications for use of Hg as a volcanic proxy. Earth Planet Sci. Lett. 543, 116333 https://doi.org/10.1016/j.epsl.2020.116333.
Shen, J., Yin, R., Zhang, S., Algeo, T.J., Bottjer, D.J., Yu, J., Xu, G., Penman, D., Wang, Y., Li, L., Shi, X., Planavsky, N.J., Feng, Q., Xie, S., 2022. Intensified continental chemical weathering and carbon-cycle perturbations linked to volcanism during the Triassic–Jurassic transition. Nat. Commun. 13, 299. https://doi.org/10.1038/s41467-022-27965-x.
Simms, M.J., Ruffell, A.H., 1989. Synchroneity of climatic change and extinctions in the Late Triassic. Geology 17, 265–268. https://doi.org/10.1130/0091-7613(1989)017.0265:SOCCAE.2.3.CO;2.
Slater, S.M., Twitchett, R.J., Danise, S., Vajda, V., 2019. Substantial vegetation response to Early Jurassic global warming with impacts on oceanic anoxia. Nat. Geosci. 12, 462–467. https://doi.org/10.1038/s41561-019-0349-z.
Sun, Y.D., Wignall, P.B., Joachimski, M.M., Bond, D.P.G., Grasby, S.E., Lai, X.L., Wang, L. N., Zhang, Z.T., Sun, S., 2016. Climate warming, euxinia and carbon isotope perturbations during the Carnian (Triassic) Crisis in South China. Earth Planet. Sci. Lett. 444, 88–100. https://doi.org/10.1016/j.epsl.2016.03.037.
Tomadin, L., Gallignani, P., Landuzzi, V., Oliveri, F., 1986. Fluvial pelitic supplies from the Apennines to the Adriatic Sea. I - The rivers of the Abruzzo Region. Mineral. Petrogr. Acta 29, 277–286.
Tomimatsu, Y., Nozaki, T., Sato, H., Takaya, Y., Kimura, J.I., Chang, Q., Naraoka, H., Rigo, M., Onoue, T., 2021. Marine osmium isotope record during the Carnian "pluvial episode" (Late Triassic) in the pelagic Panthalassa Ocean. Glob. Planet Change 197, 103387. https://doi.org/10.1016/j.gloplacha.2020.103387.
Trotter, J.A., Williams, I.S., Nicora, A., Mazza, M., Rigo, M., 2015. Long-term cycles of Triassic climate change: a new δ18O record from conodont apatite. Earth Planet Sci. Lett. 415, 165–174. https://doi.org/10.1016/j.epsl.2015.01.038.
Vervoort, P., Adloff, M., Greene, S.E., Kirtland Turner, S., 2019. Negative carbon isotope excursions: an interpretive framework. Environ. Res. Lett. 14, 085014 https://doi.org/10.1088/1748-9326/ab3318.
Xu, G., Shen, J., Algeo, T.J., Yu, J., Feng, Q., Frank, T.D., Fielding, C.R., Yan, J., Deconink, J.F., Lei, Y., 2023. Limited change in silicate chemical weathering intensity during the Permian–Triassic transition indicates ineffective climate regulation by weathering feedbacks. Earth Planet Sci. Lett. 616, 118235 https://doi.org/10.1016/j.epsl.2023.118235.
Yang, J., Cawood, P.A., Condon, D.J., Liu, J., Deng, X., Wang, J., Du, Y., Yuan, D., 2022. Anomalous weathering trends indicate accelerated erosion of tropical basaltic landscapes during the Permo-Triassic warming. Earth Planet Sci. Lett. 577, 117256 https://doi.org/10.1016/j.epsl.2021.117256.
Yang, W., Yang, J., Wang, X., Du, Y., 2012. Geochronology from Middle Triassic to Middle Jurassic detrital zircons in Jiyuan basin and its implications for the Qinling Orogen. Earth Sci. China Univ. Geosci. 37, 489–500. https://doi.org/10.3799/dqkx.2012.055.
Zhang, K., Liu, R., Liu, Z., Li, L., 2021. Geochemical characteristics and geological significance of humid climate events in the Middle-Late Triassic (Ladinian-Carnian) of the Ordos Basin, central China. Mar. Pet. Geol. 131, 105179 https://doi.org/10.1016/j.marpetgeo.2021.105179.
Zhang, P., Lu, J., Yang, M., Bond, D.P.G., Greene, S.E., Liu, L., Zhang, Y., Wang, Y., Wang, Z., Li, S., Shao, L., Hilton, J., 2022a. Volcanically-induced environmental and floral changes across the Triassic-Jurassic (T-J) transition. Front. Ecol. Evol. 10, 853404 https://doi.org/10.3389/fevo.2022.853404.
Zhang, P., Wang, P., Yang, Z., Shi, Y., Song, C., Guo, J., Dong, Q., Chen, H., 2019. Major element geochemical features of Sandaogou loess section in Jingbian County, Northern Shaanxi Province. Sci. Technol. Eng. 19, 1671–1815. https://doi.org/CNKI:SUN:KXJS.0.2019-28-066.
Zhang, P., Yang, M., Jiang, Z., Zhou, K., Xu, X., Chen, H., Zhu, X., Guo, Y., Ye, H., Zhang, Y., Shao, L., Lu, J., 2023d. Significant floral changes across the Permian-Triassic and Triassic-Jurassic transitions induced by widespread wildfires. Front. Ecol. Evol. 11, 1284482 https://doi.org/10.3389/fevo.2023.1284482.
Zhang, P., Yang, M., Lu, J., Bond, D.P.G., Zhou, K., Xu, X., Wang, Y., He, Z., Bian, X., Shao, L., Hilton, J., 2023a. End-Permian terrestrial ecosystem collapse in North China: evidence from palynology and geochemistry. Glob. Planet Change 222, 104070. https://doi.org/10.1016/j.gloplacha.2023.104070.
Zhang, P., Yang, M., Lu, J., Jiang, Z., Zhou, K., Liu, H., He, Z., Wang, Y., Bian, X., Shao, L., Hilton, J., Bond, D.P.G., 2023b. Middle Jurassic terrestrial environmental and floral changes linked to volcanism: evidence from the Qinghai-Tibet Plateau, China. Glob. Planet Change 223, 104094. https://doi.org/10.1016/j.gloplacha.2023.104094.
Zhang, P., Yang, M., Lu, J., Jiang, Z., Zhou, K., Xu, X., Wang, Y., Wu, L., Chen, H., Zhu, X., Guo, Y., Ye, H., Shao, L., Hilton, J., 2023c. Floral response to the late Triassic Carnian Pluvial Episode. Front. Ecol. Evol. 11, 1199121 https://doi.org/10.3389/fevo.2023.1199121.
Zhang, P., Yang, M., Lu, J., Shao, L., Wang, Z., Hilton, J., 2022b. Low-latitude climate change linked to high-latitude glaciation during the late Paleozoic ice age: evidence from terrigenous detrital kaolinite. Front. Earth Sci. 10, 956861 https://doi.org/10.3389/feart.2022.956861.
Zhao, H., Grasby, S.E., Wang, X., Zhang, L., Liu, Y., Chen, Z.Q., Hu, Z., Huang, Y., 2022. Mercury enrichments during the Carnian Pluvial Event (Late Triassic) in South China. GSA Bull. 134, 2709–2720. https://doi.org/10.1130/B36205.1.